

We are IntechOpen, the world's leading publisher of Open Access books Built by scientists, for scientists

5,800

Open access books available

142,000

International authors and editors

180M

Downloads

Our authors are among the

154

Countries delivered to

TOP 1%

most cited scientists

12.2%

Contributors from top 500 universities



WEB OF SCIENCE™

Selection of our books indexed in the Book Citation Index
in Web of Science™ Core Collection (BKCI)

Interested in publishing with us?
Contact book.department@intechopen.com

Numbers displayed above are based on latest data collected.
For more information visit www.intechopen.com



Chapter

Support Strength Criteria and Intelligent Design of Underground Powerhouses

Jianhai Zhang, Tianzhi Yao, Li Qian, Zuguo Mo, Yunpeng Gao, Fujun Xue, Chenggang Liao and Zhong Zhou

Abstract

The proper design of underground powerhouse support is the key engineering technique to guarantee the safe construction and operation of underground works. By regression analysis of the surrounding rock support parameters of 29 underground powerhouses with a span of 18.0–34.0 m, the empirical formula of the relationship between the support strength of anchor bar, strength-stress ratio, and plant span and the relationship among the support strength of the anchor cable, strength-stress ratio, and plant span are proposed. Furthermore, an intelligent design model for the anchor support of the underground powerhouse was trained by a BP (back propagation) neural network. Research shows that the support strength index of the anchor bolt and the anchor cable of these 29 plants are all distributed around 1.0. Therefore, a support strength index of 0.8–1.2 can be used as a reference for practical engineering support design. Finally, the reliability of the intelligent design model for the anchor support of the underground powerhouse was verified by comparison with actual engineering and support strength index. This shows that the intelligent design model can provide a reference for engineering design and construction.

Keywords: underground powerhouse, support strength criteria, strength-stress ratio, BP neural network, intelligent design

1. Introduction

The underground plant of a hydropower station is a large, complex underground building structure, and its stability is affected by factors such as geological structure, carved span, in situ stress, and support strength [1]. As underground plants are located in different stress environments, the lithology and strength of the surrounding rock are different, and the strength of the support to maintain the stability of the surrounding rock varies. Insufficient support strength can lead to local instability, collapse, excessive deformation of the surrounding rock, or even integral damage,

while too much support strength can lead to unnecessary waste. Due to the complexity of the surrounding rock, scholars are still unable to fully grasp the deformation characteristics and reinforcement mechanism of the surrounding rock under complex stress conditions, which makes the theory and specification of surrounding rock reinforcement immature, and the support of underground plants still mainly relies on experience for design and construction. At present, the support design of underground plants is commonly based on the engineering analogy method, and there is insufficient knowledge of the deformation characteristics of the surrounding rock in high in situ stress areas. Because of the lack of relevant design experience, it is not sufficient to fully guide the design of the cavern support. The empirical method sometimes leads to safety problems due to inadequate design support strength or waste of resources due to over-support.

On the other hand, many successful examples of underground plants provide valuable data for the design of rock support. Through these data, the reinforcement measures and strength of the surrounding rock can be summarized, and the inherent laws of rock support and a new support design method can be proposed. For underground plants, the commonly used method is the system anchor and anchor cable support method, which can give good play to the strength and its own bearing capacity of the surrounding rock [2]. Through studying research papers and design data, a systematic summarization of sidewall support schemes for 29 underground plants with a span range of 18.0–34.0 m and a strength-stress ratio range of 2.0–14.55 was carried out, and the regression fitting relationships between the strength of the system anchor bolts and cables and the strength-stress ratio of the surrounding rock and the plant span were proposed. Based on the regression fitting relationship, an underground plant support strength index was defined, which can quantitatively evaluate whether the surrounding rock support is reasonable.

Neural network theory is recognized as a method for solving nonlinear problems, and it has been applied in rock mechanics parameter identification and stress analysis, parameter prediction, rock stability, rock deformation prediction, and rock engineering inverse analysis [3, 4]. One of the most popularly used neural network models is BP (back propagation) neural networks, which are multilayer feed-forward neural networks that are widely used in nonlinear modeling, function approximation, logic classification, etc. On this basis, an intelligent design model for the anchor support of the underground powerhouse is proposed based on a BP neural network. The model optimized the design of the system anchor diameter and spacing by inputting the plant span and strength-stress ratio. The different degrees of influence of the plant span and strength-stress ratio on the system anchor support scheme were analyzed according to the weights between the neurons.

1.1 Underground plant and rock surrounds support

1.1.1 Underground plant

According to incomplete statistics, more than 600 underground hydropower plants have been built worldwide, including more than 200 in Norway, which is the largest number of underground hydropower plants, and there are two underground power plants with an installed capacity of more than 1000 MW. As of 2015,

the top 10 underground hydropower plants of installed capacity that have been built in the world are shown in **Table 1**.

The underground plant caverns are generally located in the hills downstream of the dam, mainly consisting of the diversion cavity, underground plant, traffic cavity, transformer room, surge chamber, and tailwater cavity, as shown in **Figure 1**. When designing the location of the plant, the longitudinal axis of the plant should have a small angle to the direction of the maximum principal stress of the initial ground stress and a large angle to the main structural surface, which is conducive to the stability of the cavern envelope.

Number	Name	Country	Installed capacity/ MW	Size of underground plant (L*W*H)/m	Completion date
1	Xiluodu	China	13,860	439.7*31.9*75.6	2014
2	Longtan	China	6300	388.5*30.3*74.5	2009
3	Nuozhadu	China	5850	418.0*29.0*79.6	2014
4	La Grande II	Canada	5280	490.0*26.3*47.2	1980
5	Churchill Falls	Canada	5225	300.0*24.5*45.5	1971
6	Jinping II	China	4800	352.4*28.3*72.2	2014
7	Sanxia	China	4200	311.3*32.6*87.3	2009
8	Xiaowan	China	4200	298.4*30.6*79.3	2012
9	Laxiwa	China	4200	311.7*30.0*73.8	2011
10	Jinping I	China	3600	277.0*28.9*68.8	2014

Table 1.
 Top 10 installed capacity underground hydropower plants in the world.

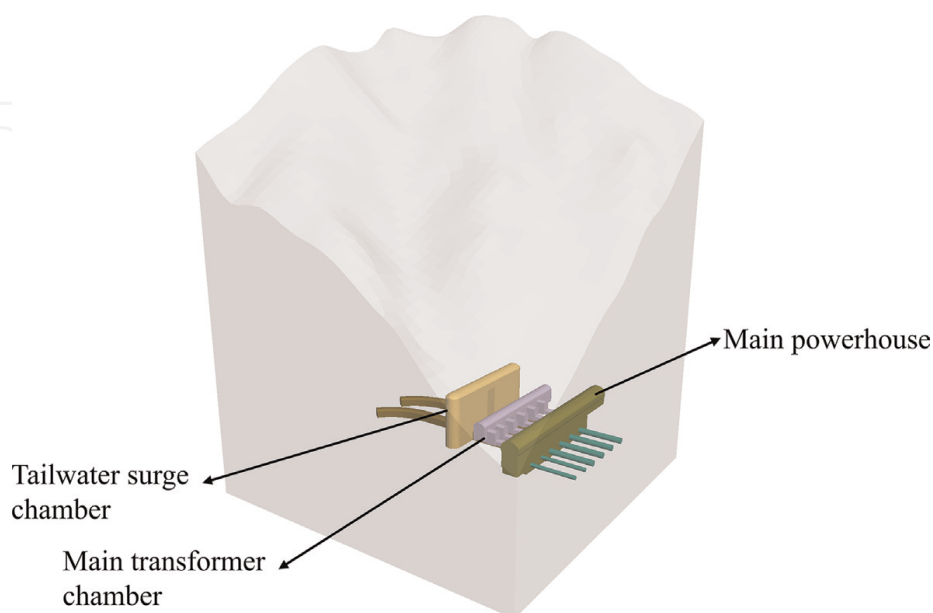


Figure 1.
 Composition of the underground plant of hydropower station.

2. The effect of anchoring measures on the parameters of surrounding rock

2.1 Effect of anchor on the parameters of the surrounding rock

At present, numerical calculations generally take the anchor bolt (anchor cable) as the rod element, and the effect of the anchor bolt is reflected by the stiffness of the anchor, which is very small compared to the stiffness of the surrounding rock. Many calculations have shown that this method of simulation does not fully reflect the support effect of the anchor bolts. In fact, the main role of the anchor is to participate in the deformation process of the surrounding rock. The elastic recovery deformation of the anchor has a reverse locking force, which can create an anchoring effect on the surrounding rock. In other words, the deformation and strength parameters of the anchored rock mass can be increased and have been confirmed by laboratory and field tests [5].

For the strength of the surrounding rock after anchoring, the parameters for the shear strength of the surrounding rock after the anchor is applied can be calculated as:

$$\begin{aligned} C_1 &= C_0 + \eta \frac{\tau_s S}{ab} \\ \varphi_1 &= \varphi_0 \end{aligned} \quad (1)$$

where C_0 and φ_0 are the cohesion and angle of internal friction of the surrounding rock before anchoring, respectively; τ_s is the shear strength of the anchor bolt; S is the cross-sectional area of the anchor bolt; a and b are the spacing and row spacing of the anchor arrangement, respectively; and η is the anchor group effect factor, which is dimensionless and is related to factors such as the anchor diameter, generally taken as $\eta = 2.0 \sim 5.0$. Eq. (1) shows that the improvement of the parameters of the surrounding rock by the anchor is mainly manifested by an increase in cohesion, and the increase in cohesion after the application of the anchor is as follows:

$$\Delta C_b = \eta \frac{\tau_s S}{ab} = \eta \tau_s \frac{\pi d^2}{4ab} \quad (2)$$

where d is the diameter of the anchor.

2.2 Incremental cohesion of the surrounding rock for anchor cable reinforcement

The traditional anchor reinforcement mechanism considers the reinforcing effect of anchor cables as (1) keeping separated rock masses from falling off and (2) increasing the overall strength by rebounding the damaged rock masses. The anchor cable not only has the above effect but also exerts a positive pressure on the rock in the direction of the anchor. This is equivalent to increasing the lateral pressure of the surrounding rock, which changes the rock near the excavation face from a one-dimensional stress state to a three-dimensional stress state and increases the strength of the surrounding rock.

As shown in **Figure 2**, the state of the point on the free surface is one-dimensional pressure, that is, $\sigma_1 > 0$, and $\sigma_3 = 0$, corresponding to Mohr's circle **O**. The increase in wall pressure and the decrease in the radius of Mohr's circle after the application of the

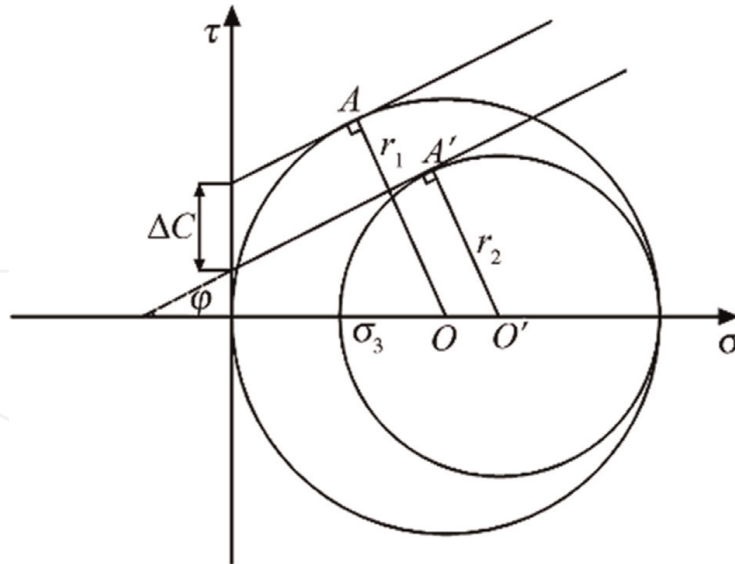


Figure 2.
 Reinforcement mechanism of anchor cable.

prestress leads to a decrease in the tangent point of Mohr's circle from A to A', which corresponds to an intercept difference ΔC with the τ -axis of the shear stress and is taken as the incremental cohesion ΔC_p of the surrounding rock provided by the anchor cable.

Assuming that the coefficient of friction $f = \tan\phi$ of the rock mass is constant before and after reinforcement, it can be deduced from **Figure 2** that the cohesion of the rock mass can be increased by applying a prestressing force N (kN) with spacing a (m) and row b (m):

$$\Delta C_p = \eta \frac{Nf}{2ab} \left(1 + \frac{1}{\sin\phi} \right) \quad (3)$$

Similar to Eq. (1), the anchor group effect factor $\eta = 2.0 \sim 5.0$, where ϕ is the internal friction angle of the surrounding rock before anchoring.

2.3 Comparison of the stability of the surrounding rock with and without support

Systematic support has a very significant effect on maintaining the stability of the surrounding rock during excavation. Taking the Yebatan hydropower station as an example, the distribution characteristics of the large deformation zones in the surrounding rock with and without system support were compared based on the FLAC^{3D} calculation software. The deformation distribution characteristics of the main powerhouse, main transformer chamber, and tailwater surge chamber under unsupported and systematically supported are shown in **Figures 3–10**. The comparison shows that:

1. The maximum local deformation of the roof arch of the main powerhouse is reduced from 70 ~ 130 mm to 60 ~ 80 mm and the maximum local deformation of the side walls is reduced from 120 ~ 180 mm to 100 ~ 150 mm under systematic support.

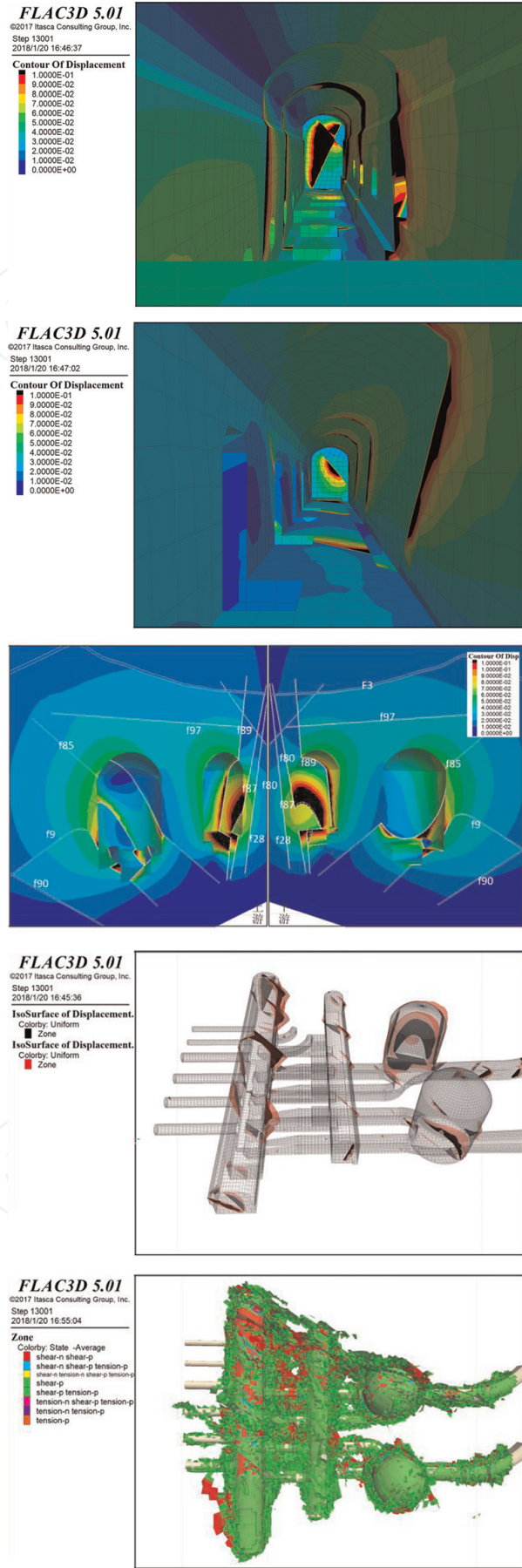


Figure 3. Distribution characteristics of the deformation (black >100 mm) of the main powerhouse under unsupported conditions.

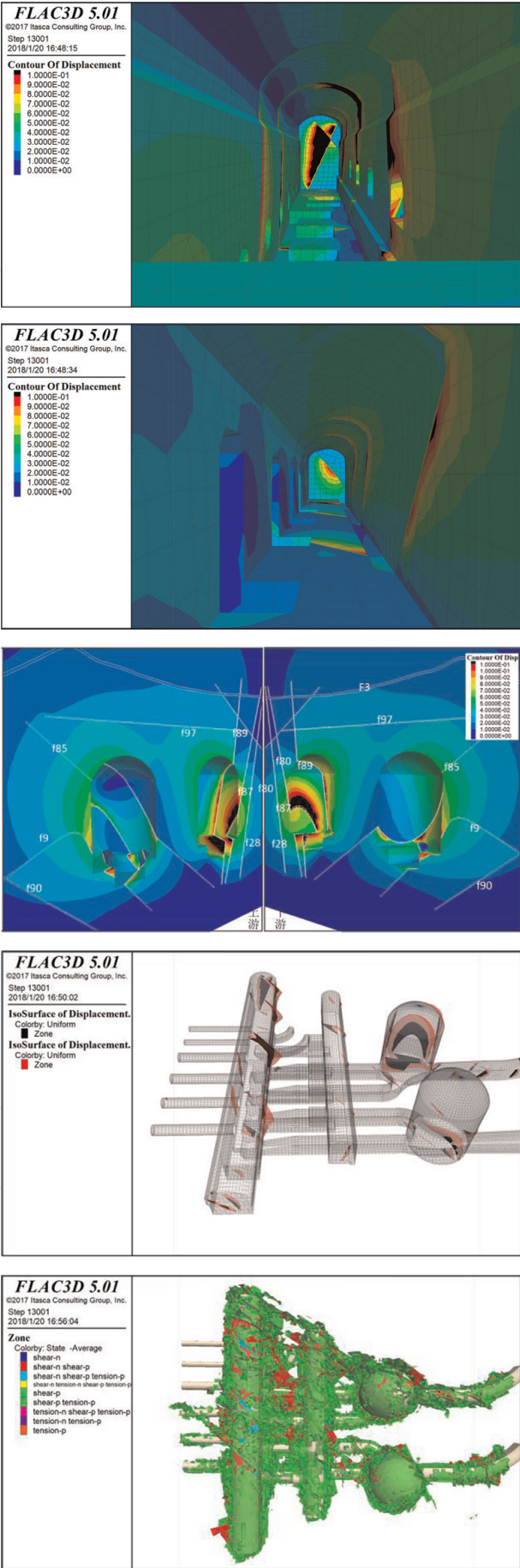


Figure 4. Distribution characteristics of the deformation (black >100 mm) under systematic support conditions.

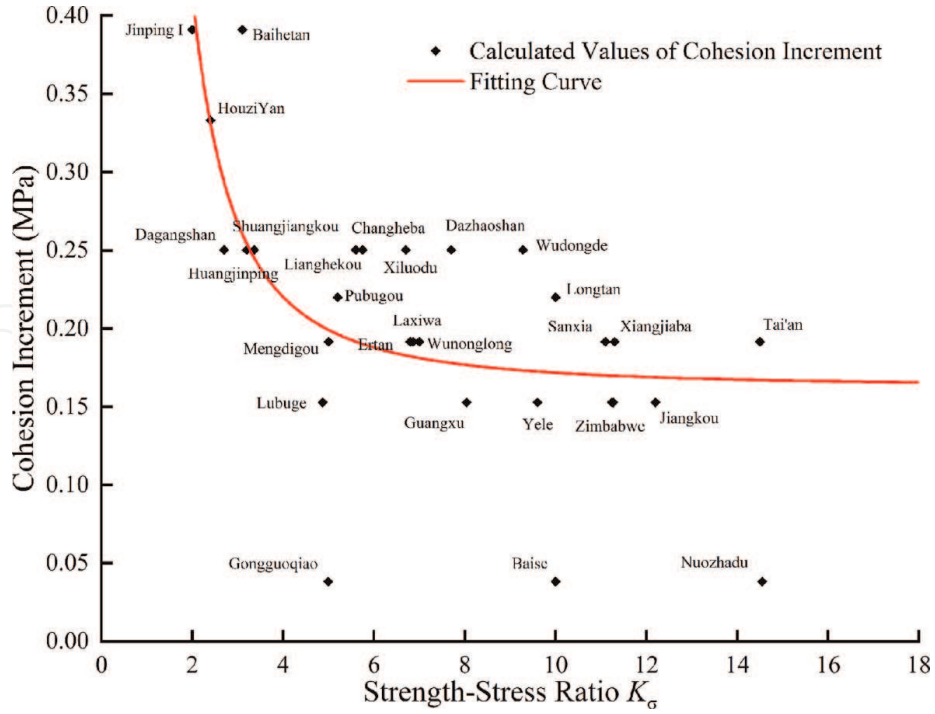


Figure 5. Relationship between cohesion increment of the anchor bolt and strength stress ratio.

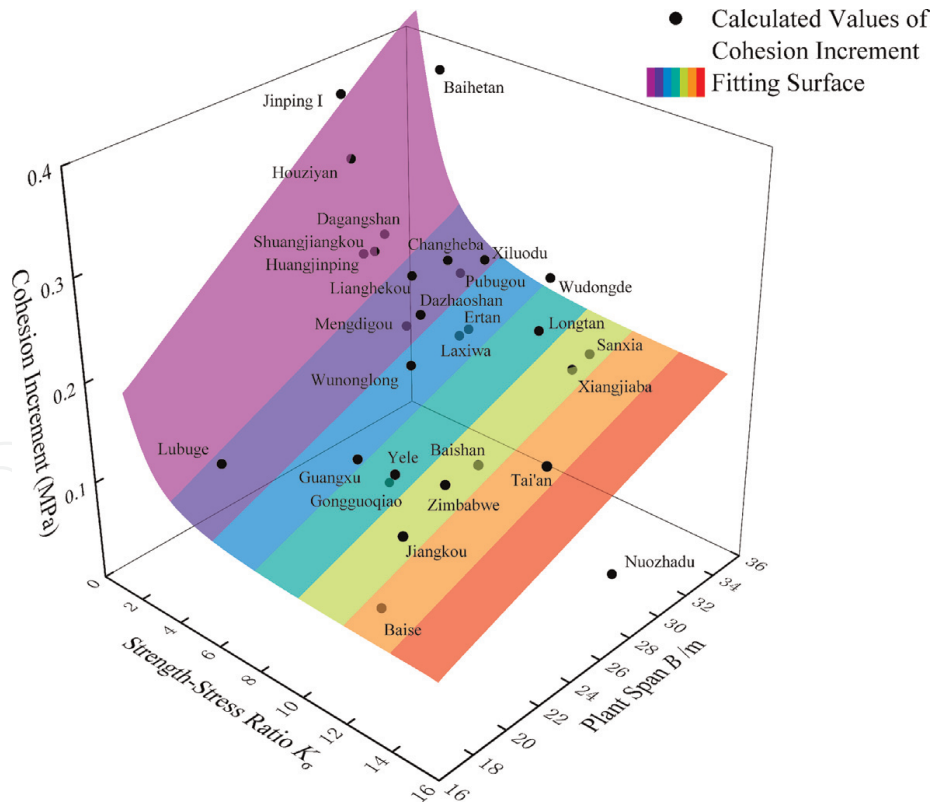


Figure 6. Relationship between cohesion increment reinforced by anchor, strength-stress ratio, and plant span.

2. The maximum local deformation of the roof arch of the main transformer chamber is reduced from 65 ~ 85 mm to 50 ~ 60 mm; the maximum local deformation of the side walls is reduced from 90 ~ 135 mm to 70 ~ 110 under the systematic support.

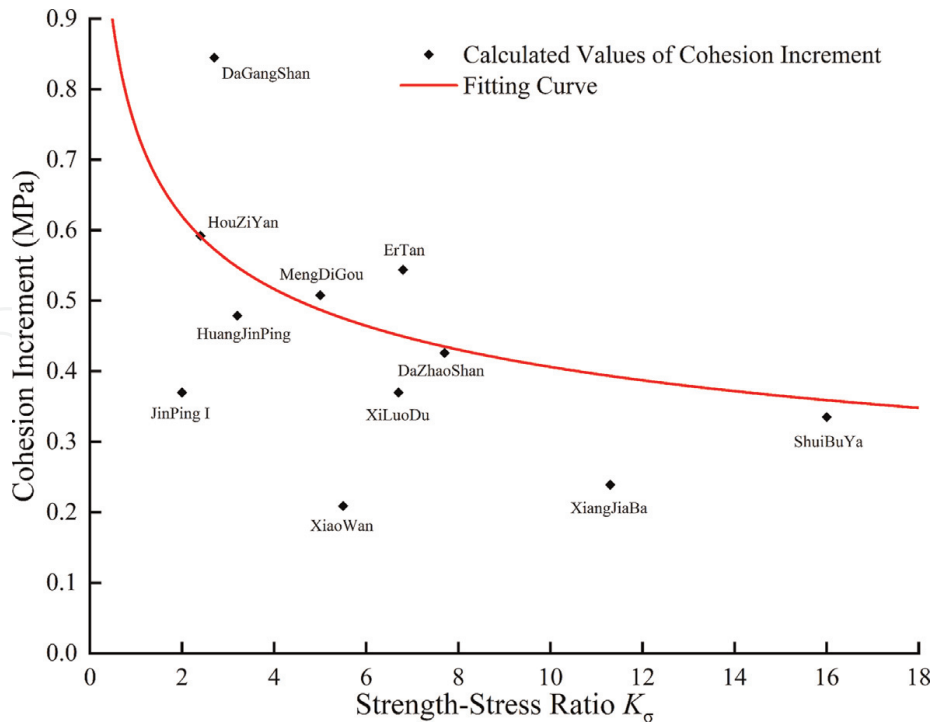


Figure 7.
 Relationship between cohesion increment reinforces by anchor cables and strength-stress ratio.

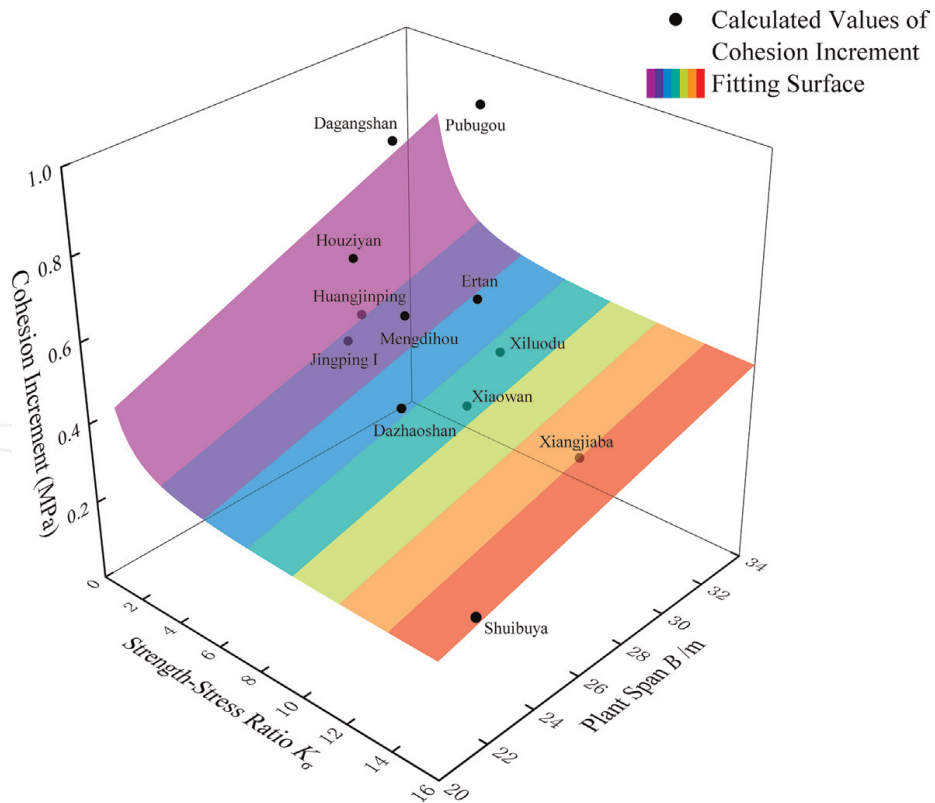


Figure 8.
 Relationships among cohesion increment reinforce by anchor cable, strength stress ratio, and plant span.

3. The maximum local deformation of the roof arch of the tailwater surge is reduced from 80 ~ 110 mm to 70 ~ 105 mm, the maximum local deformation of the side walls is reduced from 100 ~ 170 mm to 100 ~ 130 mm. under the system support.

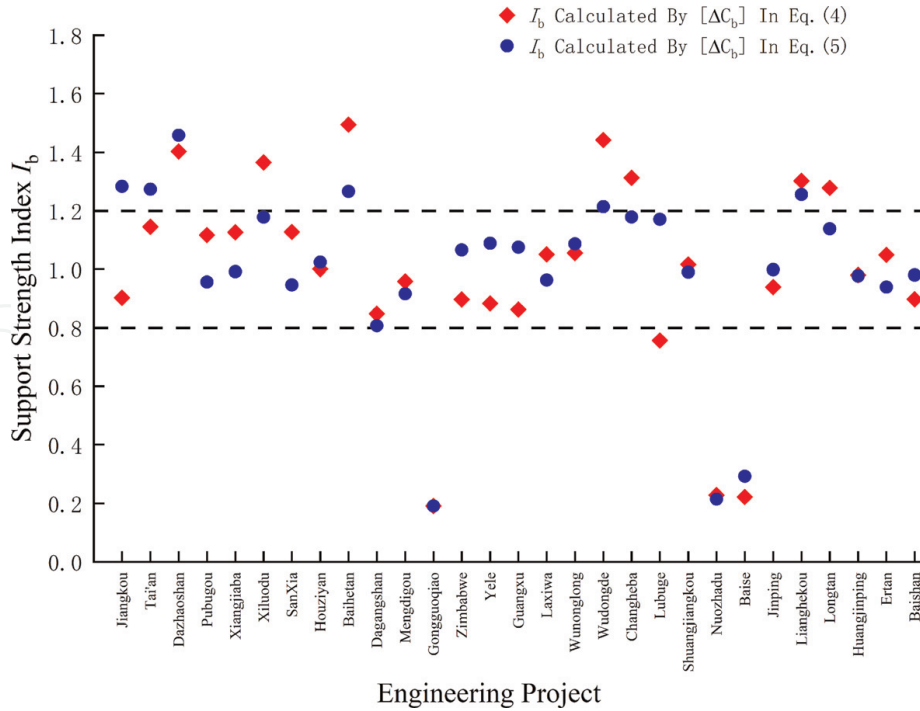


Figure 9. Comparison of anchor bolt support index calculated by different fitting formulas.

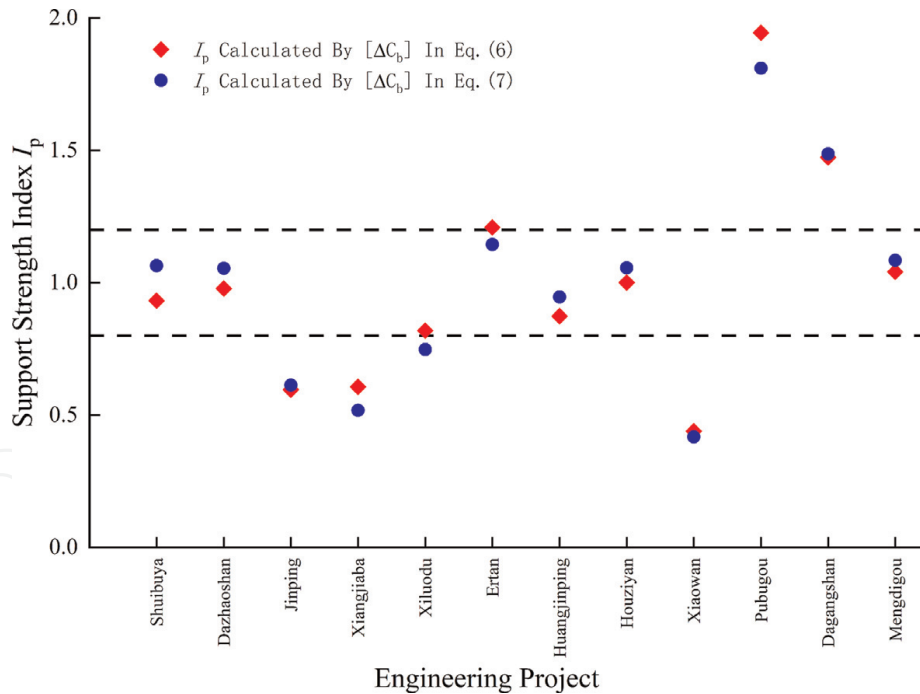


Figure 10. Comparison of anchor cable support index calculated by different fitting formulas.

4. Under system support, the volume of the cavern group surrounding rock deformation greater than 100 mm is reduced from 21.6 to 9.7 thousand cubic meters.

In general, the deformation distribution characteristics of the surrounding rock under system support are similar to those under unsupported, but the extent and magnitude of large deformations at fault-affected areas are substantially reduced under system support.

3. Relationship among the plant span, strength-stress ratio, and incremental cohesion of the surrounding rock

3.1 Incremental cohesion of the surrounding rock after anchor reinforcement

As shown in **Table 2**, the physical and mechanical parameters, maximum principal stress, and anchor parameters of the underground plants of 29 hydropower stations, such as Jiangkou, Xiluodu, and Jinping I, are shown [6–36]. In **Table 2**, the maximum principal stress is taken as the maximum value near the main powerhouse. In accordance with the design principle of the “difference between arch and side wall”, generally, the system anchors on the side wall of the main plant are used for statistical data. When the system anchor arrangement for the upstream and downstream side walls varies, the average value is taken as the statistical data. The incremental cohesion of the surrounding rock is calculated by Eq. (2), where $\eta = 3.5$, $\tau_s = 200$ MPa, and the strength-stress ratio in **Table 2** is a dimensionless constant.

3.1.1 Relationship between the cohesion increment and strength-stress ratio of surrounding rock

The strength-stress ratio and cohesion increment of the 29 underground plants in **Table 2** are plotted as 29 data points in **Figure 5**. These data are fitted by a least-squares curve to obtain Eq. (4).

$$[\Delta C_b] = 0.45(2K_\sigma^{-2} + K_\sigma^{-4}) + 0.163 \quad (4)$$

As shown in **Figure 5**, most of the 29 data points are distributed near the fitted curve, forming a data band around a certain distance above and below the curve, and the cohesion increment of the surrounding rock increases with a decrease in the strength-stress ratio. The trend of the curve in **Figure 5** shows that when the strength-stress ratio $K_\sigma > 6.0$, the support strength reflected by the cohesion increment of the surrounding rock gradually tends to be constant. However, when the strength-stress ratio ranges from $3.0 \leq K_\sigma < 6.0$, the curve gradually rises, indicating that the required support strength of the surrounding rock increases significantly as the strength-stress ratio decreases. When the strength-stress ratio $K_\sigma < 3$, the underground plant surrounding rock is in a high-very high-stress state, requiring an even higher support strength, and the cohesion increment ΔC_b and strength-stress ratio show -2 times nonlinearity. Eq. (4) shows that the smaller the strength of the surrounding rock and the higher the in situ stress of the underground plant are, the greater the support strength required, but the growth rate shows a nonlinear relationship with the strength-stress ratio.

3.1.2 Relationship between the cohesion increment and the strength-stress ratio and plant span

According to the 29 underground plants in **Table 2**, the cohesion increment ΔC_b of the surrounding rock is fitted to the plant span B and the strength-stress ratio K_σ by least squares surface fitting, and the equation is as follows:

$$[\Delta C_b] = 0.01481(2K_\sigma^{-2} + 0.405)B \quad (5)$$

Engineering	Cavern span/m	Uniaxial compressive strength/MPa	Maximum principal stress/MPa	Strength-stress ratio K_σ	Anchor diameter D /mm	Anchor spacing and row spacing a, b /m	Calculated values of cohesion increments ΔC_b /MPa
Jiangkou	19.2	90	7.40	12.2	25.0	1.5	0.153
Tai'an	24.5	160	11.0	14.5	28.0	1.5	0.192
Dazhaoshan	26.4	85	11.0	7.70	32.0	1.5	0.250
Pubugou	32.4	120	23.3	5.20	30.0	1.5	0.220
Xiangjiaba	31.0	100	8.90	11.3	28.0	1.5	0.192
Xiluodu	31.9	120	18.0	6.70	32.0	1.5	0.250
SanXia	32.5	130	11.7	11.1	28.0	1.5	0.192
Houziyan	29.2	80	33.5	2.40	32.0	1.3	0.333
Baihetan	34.0	95	31.0	3.10	32.0	1.2	0.391
Dagangshan	30.8	60	22.2	2.70	32.0	1.5	0.250
Mengdigou	29.1	85	17.0	5.00	28.0	1.5	0.192
Gongguoqiao	27.8	70	14.0	4.99	25.0	3.0	0.038
Zimbabwe	23.0	100	8.90	11.24	25.0	1.5	0.153
Yele	22.2	120	12.5	9.60	25.0	1.5	0.153
Guangxu	22.0	112.5	14.0	8.04	25.0	1.5	0.153
Laxiwa	30.0	157.0	22.87	6.86	28.0	1.5	0.192
Wunonglong	26.7	70.0	10.0	7.00	28.0	1.5	0.192
Wudongde	32.5	90.0	9.70	9.28	32.0	1.5	0.250
Changheba	30.8	138	24.0	5.75	32.0	1.5	0.250
Lubuge	18.0	82.8	17.0	4.87	25.0	1.5	0.153
Shuangjiangkou	29.3	97.3	29.0	3.36	32.0	1.5	0.250
Nuozhadu	29.0	120.3	8.27	14.55	25.0	3.0	0.038
Baise	20.7	60.0	6.00	10.00	25.0	3.0	0.038
Jinping I	29.2	70	35.7	2.00	32.0	1.2	0.391
Lianghekou	28.7	100	18.0	5.60	32.0	1.5	0.250
Longtan	30.7	130	13.0	10.0	30.0	1.5	0.220
Huangjinping	28.8	75	23.2	3.20	32.0	1.5	0.250
Ertan	30.7	200	29.5	6.80	28.0	1.5	0.192
Baishan	25.0	108.0	9.58	11.27	25.0	1.5	0.153

Table 2. Relevant data of the powerhouse and calculation of the cohesion incrementally reinforced by the anchor bar.

In **Figure 6**, the cohesion increment provided by the anchor is approximately linearly related to plant span B , which increases with an increase in plant span. In addition, the cohesion increment ΔC_b and strength-stress ratio still show -2 times nonlinearity.

3.2 Incremental cohesion of the surrounding rock for anchor cable reinforcement

The anchor cable support parameters for 12 large and medium-sized hydropower plants are shown in **Table 3**, and the cohesion increment in the surrounding rock is calculated by Eq. (3), where $\eta = 3.5$.

3.2.1 Relationship between the cohesion increment and strength-stress ratio of the surrounding rock

The 12 points are plotted in **Figure 7** based on the strength-stress ratio and cohesion increment ΔC_p of the surrounding rock for the 12 underground plants in **Table 3**. Eq. (6) can be obtained by fitting the least squares curve to the 12 points:

$$[\Delta C_p] = 0.7445K_\sigma^{-0.2627} \quad (6)$$

As shown in **Figure 7**, the incremental cohesion ΔC_p of the surrounding rock provided by the anchor cable decreases with increasing strength-stress ratio. When the strength-stress ratio $K_\sigma \geq 4.0$, the weakening rate of the support strength gradually decreased at a certain rate. When $K_\sigma < 4.0$, the increase rate of the support strength accelerates.

A comparison of the fitting curves of the anchor bolt in **Figure 5** and the anchor cable in **Figure 7** shows the following differences: (1) There is no obvious transition zone in the fitted curve of the anchor cable; (2) When $K_\sigma < 6.0$, the upward trend of the fitted curve of the anchor cable is less than that of the anchor bolt; and (3) when $K_\sigma \geq 6.0$, the fitted curve of the anchor cable does not converge to a constant as the anchor bolt fitting curve does but decreases at a certain rate. These differences indicate that anchor cables provide greater support strength than anchor bolts and that the rate of change in anchor cable support strength with strength-stress ratio is less than that of the anchor bolts at $K_\sigma < 4.5$.

3.2.2 Relationship among the cohesion increment, strength-stress ratio, and plant span

The relationship among cohesion increments ΔC_p , plant span B , and the strength-stress ratio K_σ of the 12 underground plants are plotted in **Figure 8**. The equation can be obtained by least-squares surface fitting:

$$[\Delta C_p] = 0.00262(5.383 + 3K_\sigma^{-1} + 4K_\sigma^{-2})B \quad (7)$$

As shown in **Figure 8**, the 12 data points are distributed approximately around the fitted curve surface, and the incremental cohesion of the surrounding rock increases with the plant span, which is consistent with engineering practice. The incremental cohesion of the surrounding rock is approximately linearly related to the plant span when the strength-stress ratio is greater than a certain value.

3.3 Support strength criteria

To better reflect the relative relationship between the actual support strength and the empirical formula, the dimensionless anchor support strength index I_b is defined as follows:

Engineering project	Plant span/m	Uniaxial compressive strength/MPa	Maximum principal Stress/MPa	Strength-stress ratio K_σ	Anchor cable internal force/kN	Anchor spacing a/m	Anchor row spacing b/m	Calculated values of cohesion increments ΔC_p /MPa
Shuibuya	21.5	90	5.62	16.0	1500	4.2	4.5	0.335
Dazhaoshan	26.4	85	11.00	7.7	2000	4.5	5.2	0.426
Jinping I	29.2	70	35.70	2.0	1750	4.5	4.5	0.370
Xiangjiaba	31.0	100	8.85	11.3	1500	5.0	6.0	0.239
Xiluodu	31.9	120	18.00	6.7	1750	4.5	4.5	0.370
Ertan	30.7	200	29.54	6.8	1500	3.0	2.0	0.544
Huangjinping	28.8	75	23.23	3.2	1750	4.0	4.0	0.479
Houziyan	29.2	80	33.45	2.4	2500	4.0	4.0	0.592
Xiaowan	31.5	140	25.40	5.5	1000	5.0	5.0	0.209
Pubugou	32.4	120	23.30	5.2	2000	3.0	3.0	0.939
Dagangshan	30.8	60	22.90	2.7	1800	4.5	4.5	0.845
Mengdigou	29.1	85	17.00	5.0	2000	4.5	4.5	0.508

Table 3.

Relevant data of each powerhouse and calculations of the cohesion increment reinforced by the anchor cable.

$$I_b = \frac{\Delta C_b}{[\Delta C_b]} \quad (8)$$

where the numerator is the calculated value of the design anchor support strength, which is calculated by Eq. (2); and the denominator is the support strength calculated by empirically fitting Eqs. (4) or (5).

Engineering	Calculated cohesion increment ΔC_b /MPa	Values calculated by Eq. (4) $[\Delta C_b]$ /MPa	Values calculated by $[\Delta C_b]$ of Eq. (4) I_b	Values calculated by Eq. (5) $[\Delta C_b]$ /MPa	Values calculated by $[\Delta C_b]$ of Eq. (5) I_b
Jiangkou	0.153	0.169	0.90	0.119	1.28
Tai'an	0.192	0.167	1.15	0.150	1.27
Dazhaoshan	0.250	0.178	1.40	0.172	1.46
Pubugou	0.220	0.197	1.12	0.230	0.96
Xiangjiaba	0.192	0.170	1.13	0.193	0.99
Xiluodu	0.250	0.183	1.37	0.212	1.18
SanXia	0.192	0.170	1.13	0.203	0.95
Houziyan	0.333	0.333	1.00	0.325	1.02
Baihetan	0.391	0.262	1.49	0.309	1.27
Dagangshan	0.250	0.295	0.85	0.310	0.81
Mengdigou	0.192	0.200	0.96	0.209	0.92
Gongguoqiao	0.038	0.200	0.19	0.200	0.19
Zimbabwe	0.153	0.170	0.90	0.143	1.07
Yele	0.153	0.173	0.88	0.140	1.09
Guangxu	0.153	0.177	0.86	0.142	1.08
Laxiwa	0.192	0.182	1.05	0.199	0.96
Wunonglong	0.192	0.182	1.06	0.176	1.09
Wudongde	0.250	0.174	1.44	0.206	1.21
Changheba	0.250	0.191	1.31	0.212	1.18
Lubuge	0.153	0.202	0.76	0.130	1.17
Shuangjiangkou	0.250	0.246	1.02	0.253	0.99
Nuozhadu	0.038	0.167	0.23	0.178	0.21
Baise	0.038	0.172	0.22	0.130	0.29
Jinping I	0.391	0.416	0.94	0.391	1.00
Lianghekou	0.250	0.192	1.30	0.199	1.26
Longtan	0.220	0.172	1.28	0.193	1.14
Huangjinpings	0.250	0.255	0.98	0.256	0.98
Ertan	0.192	0.183	1.05	0.204	0.94
Baishan	0.153	0.170	0.90	0.156	0.98

Table 4.
 Anchor bolt support index of the underground powerhouse calculated by Eqs. (4) and (5).

Similarly, the dimensionless anchor cable support strength index I_p can be defined as:

$$I_p = \frac{\Delta C_p}{[\Delta C_p]} \quad (9)$$

where the numerator is the calculated value of the design anchor cable support strength, which is calculated by Eq. (3); and the denominator is the support strength calculated by empirically fitting Eqs. (6) or (7).

The cohesion increment of the anchor cable are calculated by Eqs. (4) and (5) and the anchor cable support strength index calculated by Eq. (8) for each engineering are shown in **Table 4**. **Figure 9** shows the comparison between I_b calculated by $[\Delta C_b]$ of Eq. (4) and I_b calculated by $[\Delta C_b]$ of Eq. (5). It can be seen from **Figure 9** that (1) the anchor bolt support index I_b is mostly distributed at approximately 1.0, in which 68.96% of I_b calculated by Eq. (5) and 65.51% I_b calculated by Eq. (4) are between $0.8 \sim 1.2$; and (2) I_b calculated by Eq. (5) is closer to 1 than I_b calculated by Eq. (4). This shows that Eq. (5), which considers both the plant span and the strength-stress ratio, can better reflect the support strength of the anchors.

The cohesion increment of the anchor cable calculated from Eqs. (6) and (7) for each engineering project and the anchor cable support index calculated using Eq. (9) for each project are shown in **Table 5**. The comparison between I_p calculated by $[\Delta C_p]$ of Eq. (6) and I_p calculated by $[\Delta C_p]$ of Eq. (7) is shown in **Figure 7**. It can be seen from **Figure 10** that (1) the anchor cable support index I_p is mostly distributed at approximately 1.0, in which 58.3% I_b is between 0.8 and 1.2; and (2) the support indices calculated by different fitting formulas for the same engineering are similar. This shows that the empirical formula can reflect the strength of the anchor cable support well, and the fitted results of empirical Eqs. (6) and (7) are similar.

Engineering	Calculated cohesion increment ΔC_p /MPa	Values calculated by Eq. (6) $[\Delta C_p]$ /MPa	Values calculated by $[\Delta C_p]$ of Eq. (6) I_p	Values calculated by Eq. (7) $[\Delta C_p]$ /MPa	Values calculated by $[\Delta C_p]$ of Eq. (7) I_p
Shuibuya	0.335	0.359	0.93	0.315	1.06
Dazhaoshan	0.426	0.435	0.98	0.404	1.05
Jinping I	0.370	0.621	0.60	0.603	0.61
Xiangjiaba	0.239	0.394	0.61	0.461	0.52
Xiluodu	0.370	0.452	0.82	0.495	0.75
Ertan	0.544	0.450	1.21	0.475	1.14
Huangjinping	0.479	0.548	0.87	0.506	0.95
Houziyan	0.592	0.592	1.00	0.561	1.06
Xiaowan	0.209	0.476	0.44	0.500	0.42
Pubugou	0.939	0.483	1.94	0.518	1.81
Dagangshan	0.845	0.574	1.47	0.568	1.49
Mengdigou	0.508	0.488	1.04	0.468	1.08

Table 5. Anchor cable support strength index of the underground powerhouse calculated by Eqs. (6) and (7).

In summary, combined with the actual engineering and experience formula, the support strength index can be used as a reference basis and judging standard for the actual engineering support design:

$$\left. \begin{array}{ll} I_p \text{ or } I_b < 0.8, & \text{Low Support Strength} \\ I_p \text{ or } 0.8 < I_b < 1.2, & \text{Reasonable Support Strength} \\ I_p \text{ or } I_b > 1.2, & \text{High Support Strength} \end{array} \right\} \quad (10)$$

4. Intelligent design model for the anchor support of the underground powerhouse

4.1 Model design and training logic

4.1.1 Model design

As seen from Parts 2 and 3, the design of the anchor support for the underground powerhouse can be determined by the plant span and strength-stress ratio. There is a certain relationship among the plant span, strength-stress ratio, anchor diameter, anchor spacing, and row spacing. Their mapping relationship can be reflected by a back propagation (BP) neural network. The BP neural network is a multilayer feed-forward neural network that is widely used in nonlinear modeling, function approximation, logic classification, etc. Therefore, an intelligent design model for anchor support of the underground powerhouse was created, which can output diameter D , anchor spacing a , and row spacing b by inputting plant span B and strength-stress ratio K_σ . The model takes advantage of the logical classification of BP neural networks to find the mapping of plant spans and strength-stress ratio to different support schemes. By analyzing the scheme of anchor bolt support of completed underground powerhouses in **Table 1**, the anchor bolt support schemes are divided into six types, as shown in **Table 6**.

The model consists of three parts: an input layer, a hidden layer, and an output layer. The structure of the model is shown in **Figure 11**. The input layer contains the plant span and strength-stress ratio, and the output layer contains the anchor diameter, spacing, and row spacing of the anchor. The hidden layer is used to connect the input and output layers and to pass the weights of the neural network. The number of layers and nodes in the hidden layers affect the prediction results of the model. Theoretically, the greater the number of hidden layers is, the smaller the error of the prediction results, but too many hidden layers will lead to an overly complex network

Scheme number	Anchor diameter D/mm	Anchor spacing and row spacing $a, b/\text{m}$
1	32	1.2
2	32	1.5
3	30	1.5
4	28	1.5
5	25	1.5
6	25	3.0

Table 6.
 Anchor support schemes.

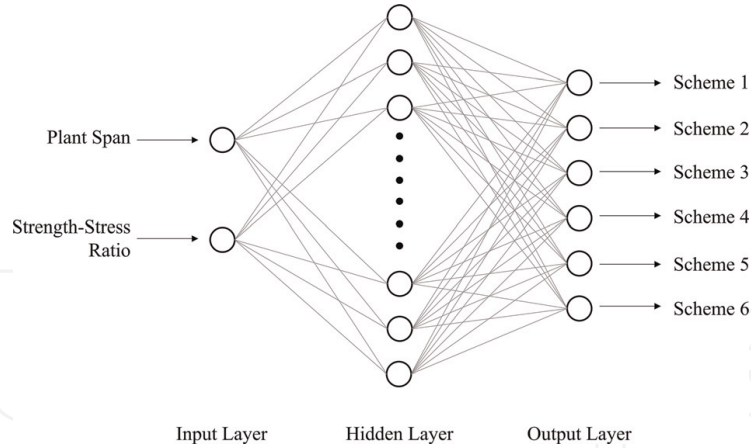


Figure 11.
The structure of BP neural network.

structure and slow computation speed. In this paper, the number of hidden layers is chosen as one layer with reference to a typical BP neural network structure. The number of nodes in the hidden layer is directly related to the number of input and output units, but there is still no perfect analytical formula. Too many nodes in the hidden layer will lead to a long learning time, while too few nodes in the hidden layer will have poor fault tolerance. According to previous experience [37], the number of nodes is designed with reference to Eq. (11).

$$m = \sqrt{n + l} + \alpha \quad (11)$$

where m is the number of nodes in the hidden layer, n is the number of nodes in the input layer, l is the number of nodes in the output layer, and α is a constant between 1 and 10. In this model, the value of α is 7, so the number of hidden layer nodes calculated according to Eq. (11) is 10.

4.1.2 Model training logic

1. Forward propagation

The initial training of the model in Step 3 of Section 4.1.2 is achieved by forward propagation of the BP neural network. Suppose the sample set is \mathbf{X} , the second layer of the BP neural network (hidden layer) is \mathbf{a}_2 , the third layer (output layer) is \mathbf{a}_3 , $\Theta^{(i)}$ is the weight from layer i to layer $(i + 1)$, the initial $\Theta^{(i)}$ is set randomly, the model target output value is \mathbf{y} , and \mathbf{h} is the actual output value of the model after training. Forward propagation can be expressed by the following equations:

$$\mathbf{a}_2 = \text{sigmoid}(\Theta^{(1)} \times \mathbf{X}^T) \quad (12)$$

$$\mathbf{a}_3 = \text{sigmoid}(\Theta^{(2)} \times \mathbf{X}^T) \quad (13)$$

$$\mathbf{h} = \mathbf{a}_3 \quad (14)$$

where \mathbf{X} , \mathbf{a}_2 , \mathbf{a}_3 , $\Theta^{(i)}$, and \mathbf{h} are the matrix and *sigmoid* is the transfer function, as shown in Eq. (15).

$$\text{sigmoid}(x) = \frac{1}{1 + e^{-x}} \quad (15)$$

2. Cost function

Because the initial $\Theta^{(i)}$ is set randomly, the actual output value \mathbf{h} of the initial model has a large error with the target output value \mathbf{y} . To evaluate the accuracy of the actual output value \mathbf{h} , the cost function $J(\Theta)$ is introduced, and the formula is shown in Eq. (16). The smaller the value of $J(\Theta)$ is, the closer the actual output value \mathbf{h} is to the target output value \mathbf{y} , representing a better value for the weight Θ .

$$J(\Theta) = -\frac{1}{m} \sum_{i=1}^m \sum_{k=1}^K \left[x_k^{(i)} \log \left(h_{\Theta} \left(x^{(i)} \right) \right)_k + \left(1 - y_k^{(i)} \log \left(1 - \left(h_{\Theta} \left(x^{(i)} \right) \right)_k \right) \right) \right] \quad (16)$$

$$+ \frac{\lambda}{2m} \sum_{l=1}^{L-1} \sum_{i=1}^{s_l} \sum_{j=1}^{s_{l+1}} \left(\Theta_{ji}^{(l)} \right)^2$$

where $x^{(i)}_k$ is the k -th data in the i -th layer, m is the total number of layers in the BP neural network, K is the total number of data, λ is a constant, L is the total number of layers in the neural network, and s_l is the number of nodes in the l -th layer.

3. Back propagation

To continuously obtain a smaller cost function $J(\Theta)$, we continuously update the value of the weight Θ by back propagation. The error transfer and weight update process are as follows:

$$\delta_k^{(3)} = \left(a_k^{(3)} - y_k \right) \quad (17)$$

$$\delta^{(2)} = \left(\Theta^{(2)} \right)^T \delta^{(3)} \times \mathbf{g}'^{(z^{(2)})} \quad (18)$$

$$\mathbf{g}'^{(z^{(2)})} = \mathbf{a}^{(2)} \times \left(1 - \mathbf{a}^{(2)} \right) \quad (19)$$

where $\delta^{(l)}_j$ is the error of the j -th node in the l -th layer and $a^{(i)}_k$ is the k -th data in the i -th layer.

The errors are stored in $\Delta^{(l)}$.

$$\Delta^{(l)} = \Delta^{(l)} + \delta^{(l+1)} \left(\mathbf{a}^{(l)} \right)^T \quad (20)$$

where $\Delta^{(l)}$ is the set of each node in l -th layer. The weight is updated with $\Delta^{(l)}$ and calculated by Eq. (20). The intelligent design model is obtained after the optimal weights are calculated.

4.1.3 Model training

The first 23 data points in **Table 1** were used as training samples to train the intelligent design model for anchor support of the underground powerhouse. The training process of the model is shown in **Figure 12**.

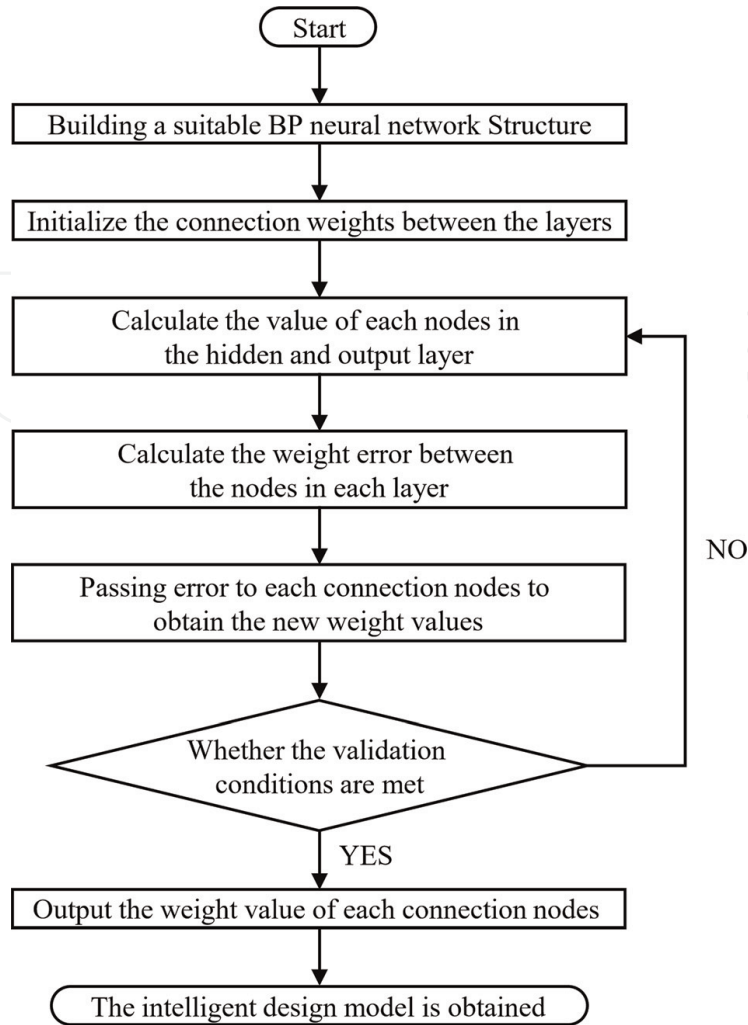


Figure 12.
The training process of BP neural network.

Step 1: A neural network structure applicable to the intelligent design model is established, as shown in **Figure 11**.

Step 2: The weight values of the neural network are initialized.

Step 3: The training set data are input. The initial training model is obtained by forward propagation of the neural network, and the values of the nodes in the neural network are obtained.

Step 4: The output layer errors of the initial training model are calculated and passed to the hidden layer to update the weights between the output layer and hidden layer. Similarly, the errors between the hidden layer and input layer are calculated, and the weights are updated.

Engineering	Plant span B/m	Uniaxial compressive strength R_c/MPa	Maximum principal stress/ MPa	Strength-stress ratio K_σ	Anchor diameter D/mm	Anchor spacing and row spacing $a, b/m$
Jinping I	29.2	70	35.7	2.00	32.0	1.2
Lianghekou	28.7	100	18.0	5.60	32.0	1.5
Longtan	30.7	130	13.0	10.0	30.0	1.5

Table 7.
Validation data.

Engineering	Plant span B/m	Uniaxial compressive strength R_c/MPa	Maximum principal stress/ MPa	Strength-stress ratio K_σ	Anchor diameter D/mm	Anchor spacing and row spacing $a, b/m$
Huangjinping	28.8	75	23.2	3.20	32.0	1.5
Ertan	30.7	200	29.5	6.80	28.0	1.5
Baishan	25.0	108.0	9.58	11.27	25.0	1.5

Table 8.
Testing data.

Step 5: After the new weights have been calculated, the new model is validated by the validation set, and if it does not meet the requirements of the validation set, then step 4 is repeated. If it does, then the final intelligent support model is obtained.

The validation set for the intelligent design model is shown in **Table 7**. The test set for the intelligent design model is shown in **Table 8**.

4.2 Model implementation

Based on the process in Section 4.1 and the data in **Table 1**, the intelligent design model was trained. Now, if the plant span and strength-stress ratio are input into the model, then the anchor diameter, spacing, and row spacing can be output. The interaction of the models can be implemented by MATLAB 2019b.

Taking the underground plant of Huangjinping Hydropower Station as an example, by inputting the plant span B and the strength-stress ratio K_σ , the model will automatically output the anchor support scheme, and the results are shown in **Figure 13**.

4.3 Model test and discussion

The test data are input in **Table 8** into the model, in turn, to obtain the support design scheme for the test set, as shown in **Table 9**.

As seen in **Table 9**, the scheme proposed by the system anchor design model for the Baishan Hydropower Station is consistent with the scheme used in actual engineering. The proposed scheme for the Ertan Hydropower Station is anchor diameter $\Phi 30$, and the anchor spacing and row spacing are $@1.5 \times 1.5$. The proposed scheme for the Huangjinping Hydropower Station is anchor diameter $\Phi 32$, and the anchor spacing and row spacing are $@1.2 \times 1.2$. The proposed schemes are safer and more reliable than the scheme used in actual engineering.

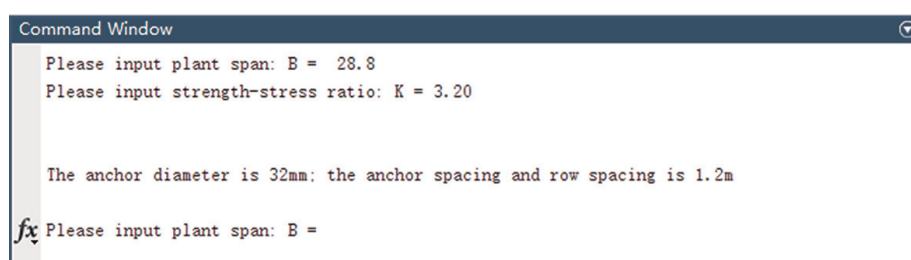


Figure 13.
Intelligent model run testing.

Engineering	Plant span B/m	Strength-stress ratio K_σ	Actual scheme of engineering	Scheme proposed by intelligent design model
Huangjinping	28.8	3.20	Anchor Diameter $\Phi 32$, Spacing and Row Spacing @1.5×1.5	Anchor Diameter $\Phi 32$, Spacing and Row Spacing @1.2×1.2
Ertan	30.7	6.80	Anchor Diameter $\Phi 28$, Spacing and Row Spacing @1.5×1.5	Anchor Diameter $\Phi 30$, Spacing and Row Spacing @1.5×1.5
Baishan	25.0	11.27	Anchor Diameter $\Phi 25$, Spacing and Row Spacing @1.5×1.5	Anchor Diameter $\Phi 25$, Spacing and Row Spacing @1.5×1.5

Table 9. Comparison between the actual scheme and the proposed scheme of the intelligent design model.

The schemes suggested by the intelligent design model are evaluated using the concept of support strength criteria presented in Section 3.3. The comparison of the proposed schemes from the intelligent design model and the actual support schemes are shown in **Figure 14**.

In high in situ stress areas, the engineering analogy method has fewer projects to provide a reliable reference for support schemes with different plant spans and strength-stress ratios. Therefore, in actual engineering, there may be a situation where the design support strength is low, such as Dagangshan Hydropower Station in Figure 15, which may cause dangerous situations during construction. In low and medium in situ stress areas, the same low strength of system anchor support was observed in Mengdigou, Baise, and Nuozhadu hydropower stations designed by the traditional method. This indicates that the engineering analogy method has difficulty

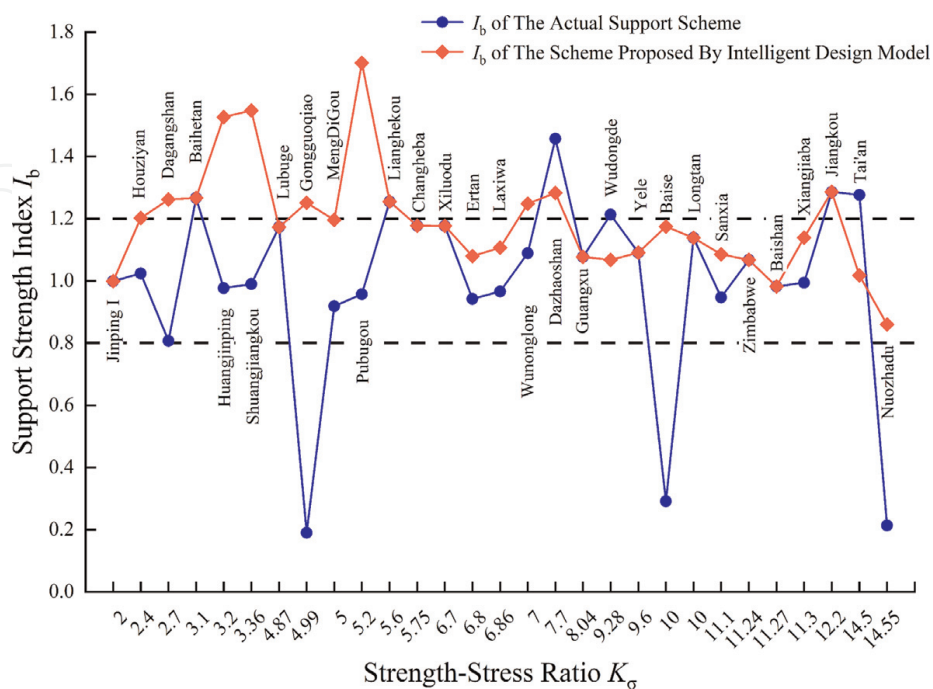


Figure 14. Comparison of the support strength index of the actual scheme and the scheme proposed by the intelligent design model.

selecting an appropriate system anchor support scheme in situations such as high in situ stress and uncommon plant spans and that the design reliability is low. However, the support strengths suggested by the intelligent design model are generally better than those used in the actual project, and generally, the support index is above 1.0. In relatively complex areas of high in situ stress, such as the Houziyan and Dagangshan hydropower stations, intelligent design models provide safer design schemes than actual engineering. This shows that the intelligent design model can provide a more reliable and economical support scheme than the traditional engineering analogy method and can be used as a reference for the design of system anchors for underground plants in practical engineering.

5. Influencing factors of support scheme design

5.1 Evaluation methods for neural network weights

The choice of a system anchor support scheme in an underground plant is influenced by several factors, but it is not yet clear which is the main factor. Based on the intelligent design model proposed above, the different degrees of influence of the plant span and strength-stress ratio on the selection of the system anchor support scheme can be further explored by analyzing the weights between the neurons. The relationship can be described with the help of the following indicators [38].

1. Correlation significance coefficient r_{ij} :

$$r_{ij} = \sum_{k=1}^p \frac{\omega_{ki}(1 - e^{-x})}{1 + e^{-x}} \quad (21)$$

$$x = \omega_{jk}$$

where i is the input unit of the neural network, $i = 1, \dots, m$; j is the output unit of the neural network, $j = 1, \dots, n$; k is the hidden unit, $k = 1, \dots, p$; ω_{ki} is the weight coefficient between neuron i in the input layer and neuron k in the hidden layer, and ω_{jk} is the weight coefficient between neuron j in the output layer and neuron k in the hidden layer.

2. Correlation index R_{ij} :

$$R_{ij} = \left| \frac{1 - e^{-y}}{1 + e^{-y}} \right| \quad (22)$$

$$y = r_{ij}$$

3. Absolute impact factor S_{ij} :

$$S_{ij} = \frac{R_{ij}}{\sum_{i=1}^m R_{ij}} \quad (23)$$

The absolute influence coefficient S_{ij} can be used to evaluate the influence of different input units on the output result, with a higher value of S_{ij} for an input unit indicating a greater influence on the result.

Input layer and hidden layer connection weights (ω_{ki})									
ω_{11}	ω_{12}	ω_{13}	ω_{14}	ω_{15}	ω_{16}	ω_{17}	ω_{18}	ω_{19}	ω_{110}
0.247	-0.263	-0.240	-0.127	-0.282	-0.263	0.266	-0.232	0.284	0.288
ω_{21}	ω_{22}	ω_{23}	ω_{24}	ω_{25}	ω_{26}	ω_{27}	ω_{28}	ω_{29}	ω_{210}
-0.662	0.305	0.664	0.173	0.241	0.303	-0.342	0.665	-0.245	-0.241
Hidden layer and output layer connection weights (ω_{jk})									
ω_{11}	ω_{12}	ω_{13}	ω_{14}	ω_{15}	ω_{16}	ω_{17}	ω_{18}	ω_{19}	ω_{110}
0.792	-0.177	-0.807	-0.043	-0.303	-0.183	0.131	-0.814	0.273	0.276
ω_{21}	ω_{22}	ω_{23}	ω_{24}	ω_{25}	ω_{26}	ω_{27}	ω_{28}	ω_{29}	ω_{210}
0.355	-0.243	-0.331	-0.059	-0.348	-0.246	0.198	-0.310	0.332	0.335
ω_{31}	ω_{32}	ω_{33}	ω_{34}	ω_{35}	ω_{36}	ω_{37}	ω_{38}	ω_{39}	ω_{310}
-0.495	-0.296	0.500	-0.100	-0.328	-0.297	0.283	0.503	0.345	0.353
ω_{41}	ω_{42}	ω_{43}	ω_{44}	ω_{45}	ω_{46}	ω_{47}	ω_{48}	ω_{49}	ω_{410}
-0.463	-0.259	0.461	-0.150	-0.030	-0.255	0.319	0.456	0.081	0.074
ω_{51}	ω_{52}	ω_{53}	ω_{54}	ω_{55}	ω_{56}	ω_{57}	ω_{58}	ω_{59}	ω_{510}
-0.267	0.236	0.259	-0.328	0.527	0.245	-0.104	0.250	-0.560	-0.520
ω_{61}	ω_{62}	ω_{63}	ω_{64}	ω_{65}	ω_{66}	ω_{67}	ω_{68}	ω_{69}	ω_{610}
-0.167	0.346	0.158	0.492	0.419	0.143	-0.597	0.157	-0.445	-0.442

Table 10.
Neural network weights of the intelligent design model.

Absolute influence coefficient S_{ij}	Scheme 1	Scheme 2	Scheme 3	Scheme 4	Scheme 5	Scheme 6
S_{ij} of plant span	0.341	0.391	0.293	0.058	0.423	0.444
S_{ij} of strength-stress ratio	0.659	0.609	0.707	0.942	0.577	0.556

Table 11.
Weight of the support scheme for the ratio of span and strength stress.

5.2 Discussion of support scheme impact factors

The weights of the neural network model in Section 4 are shown in **Table 10**.

The influence weights of the plant span and strength-stress ratio on the 6 system anchor support schemes are shown in **Table 11**.

As seen from **Table 11**, the weights of the strength-stress ratio on the results in the intelligent support design model are greater than the weights of the plant span. Therefore, when considering only the plant span and the strength-stress ratio, the variation in the strength-stress ratio has a greater influence on the choice of the anchor support scheme for the underground plant.

6. Conclusion

1. Anchor bolts or anchor cables can provide additional cohesion increments to the surrounding rock, and the support strength reflected by the anchor shows a

certain functional relationship with the strength-stress ratio and plant span. Through the statistical method of least squares fitting, four empirical formulas are proposed for the strength-stress ratio K_σ of anchor bolts and anchor cables and the plant span B .

2. For both anchor cable support and anchor bolt support, there are intervals where the strength of the support increases at a rapid rate. For anchor bolt support, the required support strength increases rapidly when the strength-stress ratio $K_\sigma \leq 3$ and the underground plant rock is in a very high-stress state; for anchor cable support, the required support strength increases significantly when $K_\sigma < 4$.
3. Based on the empirical fitting formula, a dimensionless support strength index I_b is proposed, which can visually characterize the relationship between the designed support strength and the support strength obtained from statistical analysis. The support index can be used as a reference for support design.
4. Based on the theory of BP neural networks, an intelligent design model for the anchor support of underground plant systems is proposed. Using MATLAB as the development language, the function of obtaining the system anchor support scheme by inputting the plant span and strength-stress ratio of the underground plant is realized.
5. The Huangjinping, Ertan, and Baishan hydropower stations were selected as engineering cases with high, medium, and low in situ stress conditions to verify the feasibility of the intelligent design model. Compared with actual projects, the intelligent design model provides a safer and more reliable support scheme for Huangjinping and Ertan hydropower stations.
6. With the help of the support strength index concept, the support strength of the support scheme suggested by the intelligent design model was compared with that of the scheme used in actual engineering. The results show that the support scheme suggested by the intelligent design model is safer and more stable and can still achieve the desired design effect under high in situ stress conditions.
7. By calculating the absolute influence factor S_{ij} , the weights of the strength-stress ratio and the plant span for the selection of different support schemes were obtained. Based on the calculation results, the strength-stress ratio has a greater influence on the choice of the system anchor support scheme when only the plant span and strength-stress ratio are considered. This method provides a new idea for studying the influence of different factors on the choice of system anchor support scheme.

IntechOpen

Author details


Jianhai Zhang¹, Tianzhi Yao^{1*}, Li Qian¹, Zuguo Mo¹, Yunpeng Gao¹, Fujun Xue¹, Chenggang Liao² and Zhong Zhou²

1 State Key Laboratory of Hydraulics and Mountain River Engineering, College of Water Resources and Hydropower, Sichuan University, Chengdu, China

2 Power China Chengdu Engineering Corporation Limited, Chengdu, China

*Address all correspondence to: sixonego@163.com

IntechOpen

© 2022 The Author(s). Licensee IntechOpen. This chapter is distributed under the terms of the Creative Commons Attribution License (<http://creativecommons.org/licenses/by/3.0>), which permits unrestricted use, distribution, and reproduction in any medium, provided the original work is properly cited. 

References

- [1] Ye W. Monitoring and analysis of surrounding rock stability of underground powerhouse caverns of hydropower stations. *Low Carbon World*. 2019;9(12):118-119
- [2] Liu WJ. Action mechanism and applications of surrounding rock reinforcement by grouting anchor. *Science Technology and Engineering*. 2017;17(20):270-276
- [3] Ge HW, Liang YC, Liu W, Gu XJ. Applications of artificial neural networks and genetic algorithms to rock mechanics. *Chinese Journal of Rock Mechanics and Engineering*. 2004;23(9):1542-1550
- [4] Su GS. Study on Stability Analysis and Intelligent Optimization for Large Underground Caverns under High Geostress Condition. Beijing, China: Chinese Academy of Sciences; 2006
- [5] Zhang QY, Xiang W, Zhu WS. Application of 3-D elastoplastic damage model with bolts in Xiluodu underground power house. *Chinese Journal of Computational Mechanics*. 2000;17(4):475-482
- [6] Huang ZJ, Sheng Q. Elastoplastic analysis on rockmass of the underground house in Jiangkou hydropower station. *Chinese Journal of Rock Mechanics and Engineering*. 2002;21(6):2098-2102
- [7] Cai B, Huang ZP, Liu YK. Rock mechanics experimental study of Jiangkou hydropower station. *Yangtze River*. 2001;32(3):53-55
- [8] Zhang Q, Li L, Lai DP, et al. Application of geological engineering theory to study and construction of Xiaolangdi underground plant. *Water Resources and Hydropower Engineering*. 2001;32(11):28-30
- [9] Chai ZY, Xiong W, Wang Y. Analysis of the support and deformation stability of surrounding rock in the excavation of Xiaolangdi underground power house. *Hongshui River*. 2002;21(2):36-38
- [10] Zhou HM, Ding XL, Sheng Q. Viscoelastic numerical simulation and stability evaluation on excavation process of underground power station of TGP. *Journal of Yangtze River Scientific Research Institute*. 2002;19(1):31-34
- [11] Yuan CH. Finite Element Analysis of the Stability of the Block Wall at the Downstream of the Three Gorges Underground Powerhouse. Beijing: China University of Geosciences; 2006
- [12] Xiao SR. Research on key blocks in the surrounding rock mass of underground powerhouse, the three gorges project. *Hydrogeology and Engineering Geology*. 2005;32(3):15-18
- [13] Mei SH, Sheng Q, Feng XT, Liu LP, Zhao HB. Back analysis of 3D in-situ stress field of underground powerhouse area of longtan hydropower station. *Chinese Journal of Rock Mechanics and Engineering*. 2004;23(23):4006-4011
- [14] Sun KC, Sun ZY. Stability analysis of surrounding rock mass of underground powerhouse in Xiangjiaba hydropower station. *Journal of Yangtze River Scientific Research Institute*. 2006;23(5):29-32
- [15] Deng JL, Zhao ZY, Yang YW. Underground powerhouse surrounding rock support design for Xiowan hydropower plant. *Yunnan Water Power*. 2007;23(4):55-58
- [16] Zeng J, Sheng Q, Liao HJ, Leng XL. Numerical simulation with FLAC3D on construction and excavation process of underground powerhouse of Fuziling

pumped storage hydropower station. *Rock and Soil Mechanics*. 2006;**27**(4): 638-642

[17] Tang XH, Zhang JH, Jiang F, Zhao WG, Wu ST, Zhou GF. Study on the design of reinforcement with statistical method. *Journal of Sichuan University (Engineering Science Edition)*. 2007;**39**:176-181

[18] Luo CW, Liu YF, Jing F. Three dimensional geostress test in underground plant area of Shuibuya project. *Journal of Yangtze River Scientific Research Institute*. 1999;**16**(1): 45-47

[19] Sun HY, Shang YQ, Zhang CS. Numerical modeling analysis for surrounding rockmass stability of large underground cavities. *Journal of Zhejiang University (Engineering Science)*. 2004;**38**(1):70-74

[20] Zhang DC, Zhang YM, Chen Q, Gao YH, Song XF. Excavation and support of underground caverns at Dachaoshan hydropower station. *Water Power*. 2001;**12**:32-34

[21] Zhou JP, Zhang XS, Dai QX. Rock anchor beam construction technology of Dachaoshan hydroelectric plant. *Design of Hydroelectric Power Station*. 2000; **16**(4):18-22

[22] Xue YJ, Chen SH. Two-stage analysis of geostress field for underground chamber area of Pubugou project. *Chinese Journal of Rock Mechanics and Engineering*. 2006;**25**(9):1881-1886

[23] Jiang F. *Analysis of Surrounding Rock Stability of Jinping Underground Hydropower Station*. Chengdu: Sichuan University; 2006

[24] Li L, He JD, Yu T, Fan JW. Optimization design of the longitudinal

axis of underground powerhouse. *Journal of Sichuan University (Engineering Science)*. 2003;**35**(3):34-37

[25] Zhang EB, Zhang JH, Zhao WG, Zhang LM. Study on Xiluodu hydropower station right bank underground powerhouse chamber complex stability and shear zone location sensitivity. *Design of Hydroelectric Power Station*. 2007;**23**(1):10-14

[26] Yang K, Zhang LX, Li ZK. New method for calculating geostresses in FEM analysis of underground houses. *Chinese Journal of Rock Mechanics and Engineering*. 2002;**21**(11):1639-1644

[27] Bing D, Yang K. Discussions on some general problems in 3-D non-linear FEM analysis of grouped cavern. *Journal of Wenzhou University*. 2005;**28**(2): 42-48

[28] Li SC, Chen WZ, Zhu WS. Study on stability and anchoring effect of jointed rock mass of an underground powerhouse. *Rock and Soil Mechanics*. 2003;**24**(4):510-513

[29] Zhang EB, Zhang JH, Zhou Z, Tang ZY, Wang RC. Study of unstability and support of surrounding rock in some sections of the Jinping river diversion tunnel. *Yunnan Water Power*. 2006; **22**(4):40-44

[30] Tang XH, Zhang JH, Zhang EB, Chen LM. Study on the cavern surrounding rock stability of the underground powerhouse of the Xiluodu hydropower station. *Yunnan Water Power*. 2007;**23**(1):33-37

[31] Wang JH, He RP, Wei YY. Stability analysis for surrounding rock mass of Dagangshan underground powerhouse during construction excavation. *Journal of Yangtze River Scientific Research Institute*. 2014;**31**(11):97-101

- [32] Wu K, Sheng Q, Zhang YH. Numerical simulation analysis of the excavation process of Dagangshan underground carved group. *Water Power*. 2009;35(7):20-23
- [33] Cheng LJ, Tan KQ, Zhang ZJ. Study on composite deformation failure characteristics of surrounding rocks in underground powerhouse at Changheba hydropower station. *Sichuan Water Power*. 2016;35(01):29-31+140
- [34] Wang YX. Design of underground powerhouse of Lubuge hydropower station. *Water Power*. 1998;12:44-48
- [35] Liu HY, Zhang QY, Lin B, Yu XY. Stability analysis of underground powerhouse cavern group of Shuangjiangkou hydropower station. *Yellow River*. 2009;31(08):107-109
- [36] Du FX. Study on Surrounding Rock Stability of Large-Span and High-Side Wall Underground Powerhouse of Nuozhadu Hydropower Station. Kunming, China: Kunming University of Science and Technology; 2009
- [37] Sun F, Shi XQ. Design of BP neural network based on MATLAB. *Computer and Digital Engineering*. 2007;35(08):124-126+202
- [38] Sun HJ, Wang XH. Determination of the weight of evaluation indexes with artificial neural network method. *Journal of Shandong University of Science and Technology (Natural Science)*. 2001; 20(03):84-86